CHALMERS
UNIVERSITY OF TECHNOLOGY

Aqueous mineral carbonation of three different industrial steel slags: Absorption capacities and product characterization

Environmental Research 252 (2024) 118903

Contents lists available at ScienceDirect

Environmental Research

journal homepage: www.elsevier.com/locate/envres

Aqueous mineral carbonation of three different industrial steel slags: Absorption capacities and product characterization

Emmanouela Leventaki [a], Eduarda Couto Queiroz [a], Shyam Krishnan Pisharody [a], Amit Kumar Siva Kumar [a], Phuoc Hoang Ho [a], Michael Andersson-Sarning [a], Björn Haase [b], Francisco M. Baena-Moreno [a,**], Alexandre Cuin [c], Diana Bernin [a,*]

[a] Department of Chemistry and Chemical Engineering, Chalmers University of Technology, 412 96 Gothenburg, Sweden
[b] Höganäs Sweden AB, Bruksgatan 34-35, 263 39, Höganäs, Sweden
[c] LQBin – Laboratório de Química BioInorgânica, Chemistry Department, Institute of Exact Sciences, Federal University of Juiz de Fora – UFJF, Juiz de Fora, MG, 36036-330, Brazil

ARTICLE INFO

Keywords:
Carbon capture
Transport and storage
Steel slag
Absorption capacity
Side stream utilization

ABSTRACT

Heavy carbon industries produce solid side stream materials that contain inorganic chemicals like Ca, Na, or Mg, and other metals such as Fe or Al. These inorganic compounds usually react efficiently with CO_2 to form stable carbonates. Therefore, using these side streams instead of virgin chemicals to capture CO_2 is an appealing approach to reduce CO_2 emissions. Herein, we performed an experimental study of the mineral carbonation potential of three industrial steel slags via aqueous, direct carbonation. To this end, we studied the absorption capacities, reaction yields, and physicochemical characteristics of the carbonated samples. The absorption capacities and the reaction yields were analyzed through experiments carried out in a reactor specifically designed to work without external stirring. As for the physicochemical characterization, we used solid-state Fourier Transform Infrared Spectroscopy (FTIR), X-ray diffraction (XRD), and scanning electron microscope (SEM). Using this reactor, the absorption capacities were between 5.8 and 35.3 g/L and reaction yields were in the range of 81–211 kg CO_2/ton of slag. The physicochemical characterization of the solid products with solid FTIR, XRD and SEM indicated the presence of $CaCO_3$. This suggests that there is potential to use the carbonated products in commercial applications.

1. Introduction

The energy sector and the so-called “heavy carbon industries” (i.e., cement, steel, and iron manufacturing) are responsible for most of the anthropogenic CO_2 emissions (Baena-Moreno et al., 2021; Luo et al., 2023). In particular, the iron and steel industries are the largest emitters of greenhouse gases, accounting for 8–12% of CO_2 emissions (Baciocchi et al., 2010; Gerres et al., 2021). Examples of measures that could decrease CO_2 emissions in these industries are carbon capture, utilization, and storage (CCUS) (González-Arias et al., 2022; Sabri et al., 2021; Wang et al., 2022; Yagmur Goren et al., 2024), or the production of green steel (i.e., HYBRIT project in Sweden (HYBRIT, 2023)). Nonetheless, they are still under development and far from full deployment, hence further research is required to advance these technologies and allow their large-scale implementation (International Energy Agency, 2022).

On the other hand, heavy carbon industries usually produce solid side streams that can be used, for example, as cementing materials (J. Liu et al., 2022a; Y. Liu et al., 2022b). Some of these side streams contain inorganic compounds such as CaO, MgO and other metal oxides which can react with CO_2 to form carbonates. They might also contain chemicals that are considered hazardous and thus could have adverse environmental impacts if released to the environment. Therefore, it is important to valorize these materials and ensure that they do not end up in landfill. In this context, utilizing these side streams to capture CO_2 could be a very interesting approach to reduce CO_2 emissions while simultaneously improving the management of the side streams, as displayed in Fig. 1. In fact, in a recent review of our team, we have discussed the importance of using these side streams to capture CO_2 (Baena-Moreno et al., 2022).

* Corresponding author.
** Corresponding author.
E-mail addresses: francisco.baena@chalmers.se (F.M. Baena-Moreno), diana.bernin@chalmers.se (D. Bernin).

https://doi.org/10.1016/j.envres.2024.118903
Received 28 December 2023; Received in revised form 11 March 2024; Accepted 8 April 2024
Available online 10 April 2024

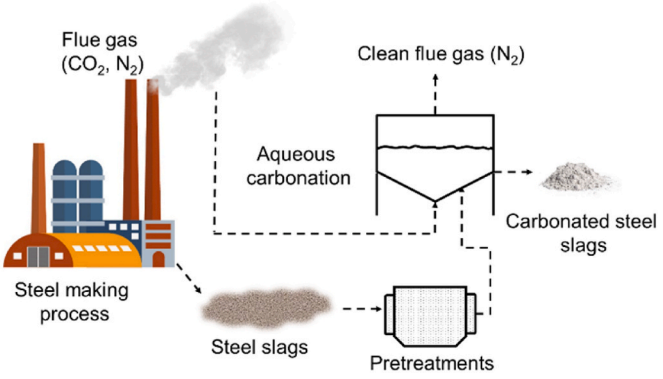

Fig. 1. Aqueous carbonation process scheme.

In the case of the iron and steel industry, the side streams produced are known as steel slags (Ragipani et al., 2021). Steel slags have already been proposed to capture CO_2 via mineral carbonation (Ragipani et al., 2021). There are two main paths for carbonation (Baena-Moreno et al., 2022): (1) Direct carbonation, which consists of a direct gas-solid reaction (dry route) or aqueous reaction (wet route) between CO_2 and the slags (Li et al., 2022). Gas-solid direct carbonation is chemically simple, but it requires high temperatures (500–700°C) to produce acceptable performances (Baena-Moreno et al., 2022). Aqueous carbonation achieves better reaction rates at mild conditions, although the reaction mechanisms are usually complex (Ho et al., 2021); (2) Indirect carbonation, which is a multi-step process that aims at extracting alkaline metals from the material and carbonating them. Indirect carbonation allows to obtain products of higher quality, but the overall costs for extraction-carbonation are high (Baena-Moreno et al., 2022).

Direct aqueous carbonation occurs in a series of steps (Luo and He, 2021). Metal ions from the solid material leach into the water until they reach their saturation point, causing a rise in the pH of the mixture. Equation (1) below describes this process, where M can be Ca or Mg. CO_2 dissolves in the alkaline medium forming CO_3^{2-} and HCO_3^- (Equations (2) and (3)) and subsequently reacts with the metal ions leading to the precipitation of metal carbonates according to Equation (4). As metal ions are consumed in this process their concentration in the aqueous medium drops below the saturation point, allowing for the dissolution of more metal ions from the solid material. Thus, the carbonation process and leaching of metal ions are in dynamic equilibrium.

$$MO_{(s)} + H_2O_{(l)} \leftrightarrow M^{2+}_{(aq)} + 2OH^-_{(aq)} \quad (1)$$

$$CO_{2(g)} + OH^-_{(aq)} \leftrightarrow HCO_3^-(aq) \quad (2)$$

$$HCO_3^-(aq) + OH^-_{(aq)} \leftrightarrow CO_3^{2-}(aq) + H_2O_{(l)} \quad (3)$$

$$M^{2+}_{(aq)} + CO_3^{2-}(aq) \rightarrow MCO_{3(s)} \quad (4)$$

CaO and MgO have a low solubility in water and the dissolution of metal ions is further hindered if they are in the form of silicate complexes (Kim and Kazonich, 2004). If the leaching of metal ions is very slow the carbonation reactions might occur on the surface of the solid particles, causing the formation of a layer of metal carbonates which hinders further dissolution of the metals. Therefore, the liquid-to-solid ratio as well as the method for wetting the solids are important parameters for enhancing the leaching of metal ions and thus optimizing the carbonation extent of these materials.

Many works have been performed previously for steel slag carbonation focusing on the study of various parameters. Accelerated carbonation with the use of 100% CO_2 in the gaseous phase has been investigated in a lot of works, such as (Chang et al., 2012; Lekakh et al., 2008; Pan et al., 2013). Less attention has been given to carbonation with lower concentrations of CO_2, more representative of industrial flue gases (Bonenfant et al., 2008; Ghacham et al., 2016). Bonenfant et al. studied the carbonation of ladle furnace slag and electric arc furnace slag with a gas flow of 15% CO_2 and 85% N_2 under ambient conditions in a slurry reactor (Bonenfant et al., 2008). They performed a series of leaching steps to enhance the carbonation capacity and concluded that ladle furnace slag had far superior carbon sequestration capacity compared to electric arc furnace slag, capturing 0.247 g of CO_2/g of slag. Ghacham et al. evaluated the effect of pressure, gas-to-liquid ratio and liquid-to-solid ratio in a batch reactor with 18.2 % CO_2 in the gas phase for ladle furnace slag (Ghacham et al., 2016). They found that the optimum conditions were 10.69 bar of pressure, 3:1 gas-to-liquid ratio and 4–10:1 liquid-to-solid ratio. Other factors that have been studied are the effect of particle size, operating temperature, reactor type, etc. as has been discussed in some review papers (Luo and He, 2021; Ragipani et al., 2021; Zhao et al., 2020). More efforts to increase the carbonation efficiency of steel slags include the use of ultrasonic waves and addition of chelating agents, such as EDTA (Luo and He, 2021; Yang et al., 2021). Ultrasonic waves transfer energy into the aqueous medium, assisting the leaching of metal ions and they have been found to yield higher metal ion leaching than mechanical stirring. The addition of EDTA in aqueous mixtures of steel slags was found to promote the leaching of Ca^{2+} and Mg^{2+} by generating H^+ in the aqueous medium and then chelating with the metal ions, leading to higher carbonation yields (Yang et al., 2021).

Table 1
Main composition (wt%) and annual production of the different steel slags.

Chemical	Petrit E	Petrit L	Petrit T
CaO	40	48	37
MgO	10	13	–
SiO_2	15	11	18
Al_2O_3	6.5	9	9
FeO	25	13	–
Fe_2O_3	–	–	7
C	–	–	20
Annual production (kton)	15–18	4–5	17–20

While there is a plethora of research around the carbonation of steelmaking slags, industrial applications still remain challenging. This fact according to Zhao et al. is caused by: (I) Differences in the composition of the slags depending on where they come from; (II) Limitation of reaction kinetics; (III) Challenges concerning energy consumption and economic costs (Zhao et al., 2020). To address these challenges and to boost the scalability of carbonation of steel slag for CO_2 capture, in this paper we evaluated the mineral carbonation potential of three different steel slags via aqueous carbonation. The three different steel slags came from Höganäs, a world leading manufacturer of metal powders for powder metallurgy based in Sweden, which gives the study a relevant industrial impact. The three steel slags come from three different points of the steel manufacturing process: (1) manufacturing of direct reduced iron (known as sponge iron); (2) ladle furnace; and (3) electric arc furnace. Their commercial names, provided by the supplier, are "Petrit T", "Petrit L", and "Petrit E" respectively, and this is how the materials will be addressed from now on. Studying three different slags might help to evaluate the suitability of each type for carbonation, hence shedding some light on the effect of different compositions. In order to fulfill challenges (II) and (III) mentioned, we performed the carbonation reactions in aqueous phase, which enhances the carbonation kinetics and thus prompts considerable energy and cost reductions since it is carried out at ambient conditions. The aim of our work is to estimate the absorption capacities of the slags, as well as to dig into the physicochemical characteristics of the carbonated product.

2. Materials and methods

2.1. Materials

Table 1 includes the composition of the three steel slags. The

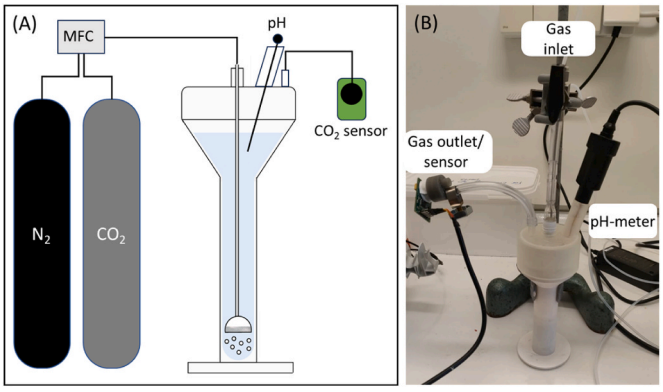

Fig. 2. (A) Scheme of the experimental setup and (B) Picture of the setup. Two gas bottles, one with CO_2 and one with N_2 were connected to an MFC where they were mixed at the ratio of 15:85 and sent to the reactor at the flow rate of 200 mL/min, a pH meter installed in the reactor measured the pH and the reactor outlet led to a CO_2 sensor.

composition is given in oxide form and the analysis was provided by Höganäs. The gas flow composition was 15% CO_2 and 85% N_2, to imitate a typical concentration of CO_2 in post-combustion flue gas. The gas flow rate was 200 mL/min.

To obtain information on the particle size of the materials SEM images were analyzed with the software FIJI (ImageJ), by measuring the dimensions of 40 particles per steel slag. For the carbonation experiments, four different Solid/Liquid (S/L) ratios were evaluated, from 50 to 200 (g/L), for the three types of slags. The mixtures were stirred before the carbonation experiments to allow the metal ions to leach into the aqueous medium. Initially, the stirring time was investigated by testing the absorption capacity of each steel slag of one S/L ratio (50) after 2 and 24 h of stirring. Then the rest of the experiments were conducted after stirring for 24 h to ensure maximum performance. To investigate the effect of the metal ions dissolution in water, control experiments were conducted where mixtures of S/L = 50 were stirred for 24 h and then centrifuged to separate the supernatants (liquid phase) from the pellets (solid phase). Subsequently, carbonation experiments were performed only on the supernatants.

2.2. Experimental setup and methodology

Fig. 2 depicts our experimental setup. The reactor was customized to avoid stirring and hence save energy while ensuring good mixing thanks to the motion of the gas bubbles. It was 3D printed with a stereolithography (SLA) 3D-printer (Form 3+, Formlabs), and designed with the software Autodesk Fusion 360. The gas bottles of CO_2 and N_2 were connected to two Mass Flow Controllers (MFC) from Brooks Instrument and the flow rate and composition of the final mixture was adjusted with a standalone controller (0254, Brooks Instrument). The gas entered the reactor through the end of the tube at the bottom. The reactor outlet was connected directly to a CO_2 sensor (ExplorIR, GSS) measuring the concentration of CO_2 every 5 s. The sensor operates with the use of a low-power LED optical technology and a nondispersive infrared (NDIR) detector tuned at the wavelength of 4.26 μm, where CO_2 has a particularly strong signal.

The experiment would be stopped once the outlet flow had the same composition of CO_2 as the inlet, meaning that CO_2 was no longer absorbed into the liquid phase. For the materials Petrit L and E, the carbonation process lasted very long, and for the most duration, the absorption of CO_2 was very small. This phenomenon will be discussed in the results section. For the sake of saving time, in such cases, the end of the experiment would be set to when the outlet flow reached 14% of CO_2. Thus, for the sake of comparison between the slags, all the graphs of Petrit T carbonation were also plotted until 14% CO_2 in the outlet unless otherwise specified. The reactor was closed with a lid to avoid gas losses and had three connections, the gas inlet, outlet and an insert spot for a pH probe (HQ430D, HACH) which was sampling the pH of the liquid phase every 10 s.

The information of the outlet gas % of CO_2 was used to obtain the rate of absorption and absorption capacity in the following way:

Knowing that the inlet flow was $F_{IN,N_2} = 200$ mL/min with 85% N_2 and since N_2 is an inert gas that is not held up in the reactor, the outlet flow of N_2 was the same as the inlet

$$F_{OUT,N_2} = F_{IN,N_2} = 200\left(\frac{mL}{min}\right)*85\% = 170\left(\frac{mL_{N_2}}{min}\right) \quad (1)$$

Thus, the total flow rate of the outlet was

$$F_{OUT,N_2} + F_{OUT,CO_2} = 170\left(\frac{mL_{N_2}}{min}\right) + F_{OUT,CO_2}\left(\frac{mL_{CO_2}}{min}\right) \quad (2)$$

Based on Equation (2), the outlet composition of CO_2 ($CO_2\%_{OUT}$) was

$$CO_2\%_{OUT} = \frac{F_{OUT,CO_2}\left(\frac{mL_{CO_2}}{min}\right)}{170\left(\frac{mL_{N_2}}{min}\right) + F_{OUT,CO_2}\left(\frac{mL_{CO_2}}{min}\right)} \quad (3)$$

Thus, the outlet flow of CO_2 (F_{OUT,CO_2}) can be expressed according to Equation (4).

$$F_{OUT,CO_2}\left(\frac{mL_{CO_2}}{min}\right) = \frac{CO_2\%_{OUT}*170\left(\frac{mL_{N_2}}{min}\right)}{1 - CO_2\%_{OUT}} \quad (4)$$

Since $CO_2\%_{OUT}$ was given every 5 s from the sensor, F_{OUT,CO_2} can be deducted from Equation (4). The density of CO_2 can be assumed to be $1.8*10^{-3}$ g/mL according to (The Engineering ToolBox (2018)), which is reasonable as the temperature measured by the pH-meter sensor was in the range of 21–23 °C for all the experiments. So, the mass of absorbed CO_2 can be calculated using Equation (5).

$$M_{absorbed\ CO_2} = \left(F_{IN,CO_2}\left(\frac{mL_{CO_2}}{min}\right) - F_{OUT,CO_2}\left(\frac{mL_{CO_2}}{min}\right)\right)*5s*\frac{1}{60}\left(\frac{min}{s}\right)*0.0018\left(\frac{g}{mL}\right) \quad (5)$$

2.3. Physicochemical characterization

Once the experiments were completed, the carbonated mixtures were dried in an oven at 50 °C for 48 h for further analysis. The solid powders were analyzed with solid state FTIR, XRD and SEM. Solid state FTIR data were obtained with attenuated total reflectance (ATR) sampling method (ATR-FTIR), using a Bruker Vertex70v instrument. Each analysis was accumulated by 64 scans in a range from 4000 to 400 cm^{-1} with a resolution of 4 cm^{-1} using RT-DLaTGS detector. XRD measurements were performed on a D8 Discover Bruker instrument. The patterns were recorded in a diffraction angle range of 2θ from 10 to 70° with a scan step of 0.02° per second. The diffractograms were recorded using the software DIFFRAC.EVA V5.2 and analyzed with the help of the

Table 2
Mean, minimum and maximum values of the particle sizes of Petrit T, L and E.

Steel slag	Mean size (μm)	Min (μm)	Max (μm)
Petrit T	7.1	0.7	63.1
Petrit L	131.6	16.8	927.0
Petrit E	250.1	5.6	1384.7

Crystallography Open Database. Additionally, the crystalline phases present in the carbonated materials were identified using the program QualX (Altomare et al., n.d.). Quantitative Phase Analysis (QPA) by Rietveld method (Paufler, 1995) was also performed using the TOPAS Academic suite program ("TOPAS-R, Version 4.2," 2009). SEM images were taken using a FEI Quanta 200 FEG ESEM instrument. Images were recorded at 20 kV using a secondary electron detector (LED). Elemental analysis by Energy Dispersive X-ray Spectrometry (EDS) was conducted on the samples after carbonation. The samples were coated with gold before the SEM analysis to increase the image quality.

3. Results

3.1. Particle size

The particle size of the three slags is presented in Table 2. Petrit T had the smallest particle size, with a mean of 7.1 μm and Petrit E had the highest mean size of 250.1 μm, while Petrit L was in between. It was decided to not crash the materials Petrit L and E into finer powders, in order to evaluate the carbonation potential of these materials as received from the industry. As will be seen in the following sections the particle size is an important factor contributing to the carbon capture efficiency of these materials.

3.2. Overview of the carbonation process

Fig. 3 shows the CO_2 percentage in the outlet of the reactor, CO_2 absorption according to the aforementioned calculations and pH over time for the S/L = 50 aqueous mixtures of Petrit T, L and E. It can be seen that for all the materials the gas outlet started with no CO_2 at time 0, but quickly sprinted to a high level once the experiment started. Plenty of information can be derived about the carbonation of the materials from these graphs. Each steel slag will be discussed separately.

For Petrit T, the outlet CO_2 concentration had an initial jump, reached the maximum of 10.3% 3.5 min into the experiment and then decreased to 9.3% within a minute before starting to increase again. Following that, in the next 10 min, the outlet CO_2 rose up to 12% and then gradually kept increasing for the next 45 min until the outlet concentration matched the inlet. All the Petrit T mixtures displayed the same pattern in the outlet CO_2 concentration. This initial spike and subsequent reduction in the outlet CO_2 could be associated with an equilibrium shift in the carbonation reactions. It could be speculated that when CO_2 is introduced into the liquid it immediately reacts with the $Ca(OH)_2$ that is dissolved in water, forming $CaCO_3$. Thus as the water is no longer fully saturated with $Ca(OH)_2$, CaO from the solid material is dissolved and immediately reacts with CO_2. This phenomenon has also been discussed in (Han et al., 2011). These inconsistencies in the outlet concentration of CO_2 were also reflected in the pH curve. The spikes in the pH curve occurred when the CO_2 concentration in the outlet exhibited slight drops, which can mean that new metal ions were dissolved increasing the pH and subsequently the CO_2 capture rate. The rate of CO_2 absorption was higher at the beginning and slowly decreased as the pH dropped.

Petrit L displayed extremely slow carbonation even at the lowest S/L ratio. At the beginning of the experiment the CO_2 outlet spiked to 12.5% within the first 6 min and 1 h after that it reached 14%, but it took another 6 h of increasingly slower CO_2 absorption until the outlet concentration reached the inlet. This also translates in the CO_2 absorption curve, as the first 0.4 g of CO_2 were absorbed within 60 min of carbonation and another 0.4 g were absorbed by the end of the experiment. The pH curve showed an initial fast drop to 9.15 after 6 min, then a jump to 10.19 within 3 min and then a downward slope after that. The lowest pH of 7.20 was reached at around 34 min and then there was a very slow rise to 7.54 at the end of the experiment. Similar pH trends have been reported before by Li et al. (2014) which studied the carbonation of $Mg(OH)_2$. According to this article, at high pH $Mg(OH)_2$ reacts with CO_2 towards the formation of $MgCO_3$ which is insoluble in water. If the surface of the undissolved MgO is covered with $MgCO_3$ then more Mg^{2+} ions cannot leach out into the water, but as CO_2 continuously

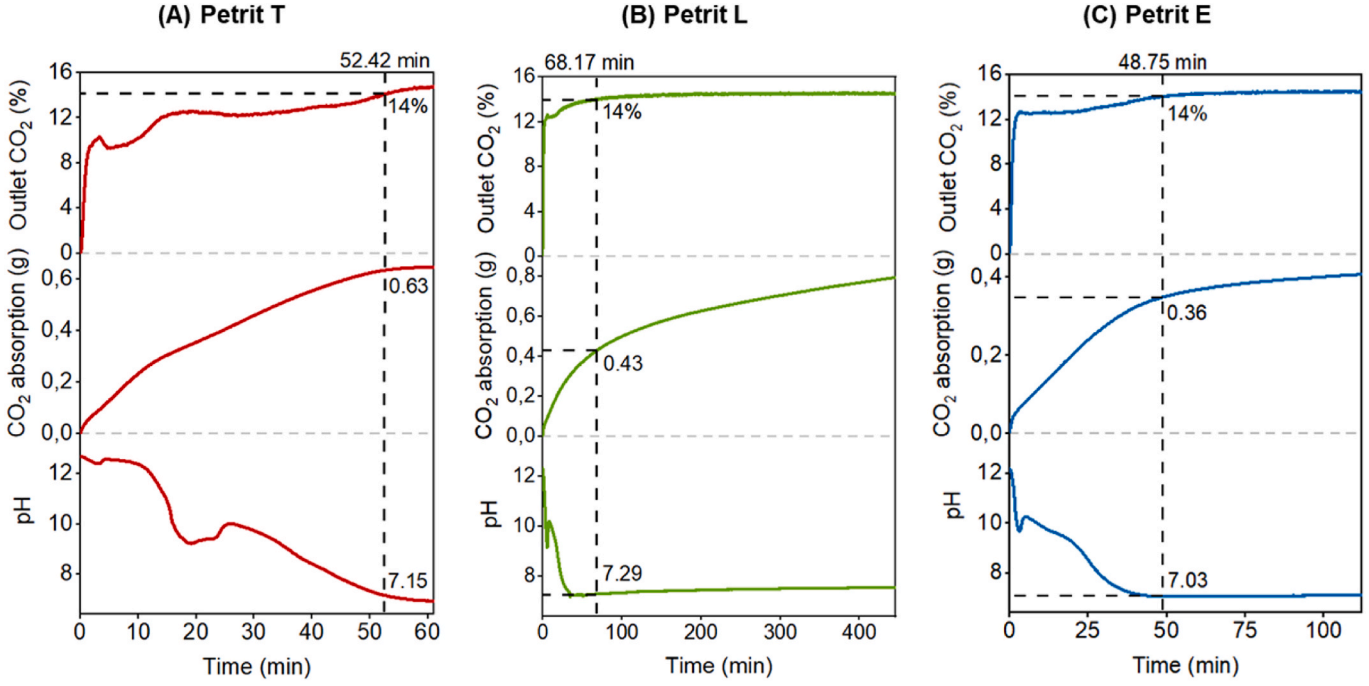

Fig. 3. Graphs of CO_2 outlet, absorption and pH with time for (A) Petrit T S/L = 50, (B) Petrit L S/L = 50 and (C) Petrit E S/L = 50.

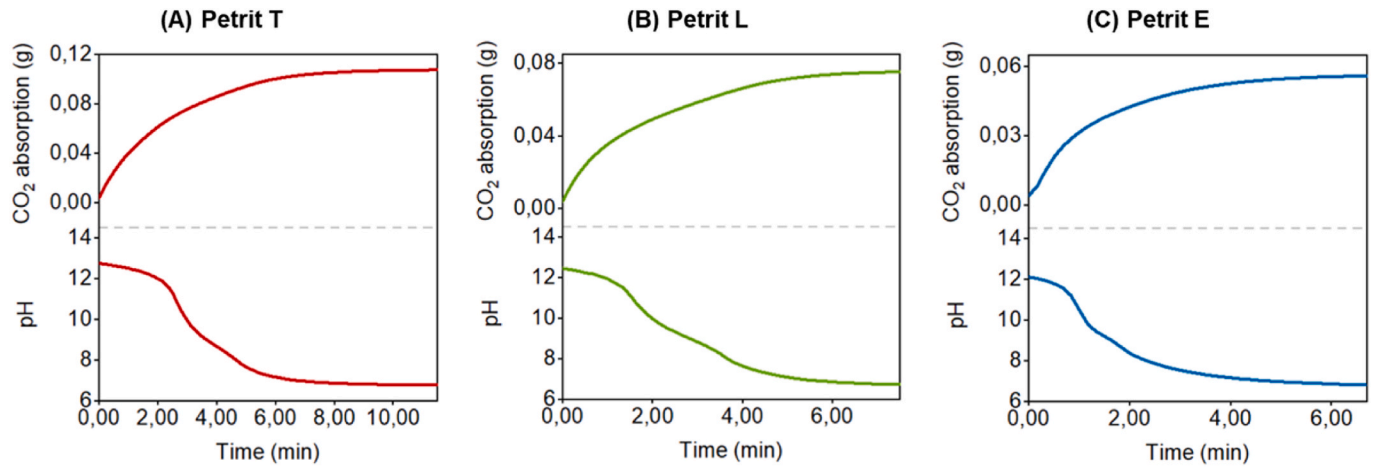

Fig. 4. Graphs of CO_2 absorption and pH with time for the filtrates of (A) Petrit T S/L = 50, (B) Petrit L S/L = 50 and (C) Petrit E S/L = 50 after stirring the mixtures for 24 h.

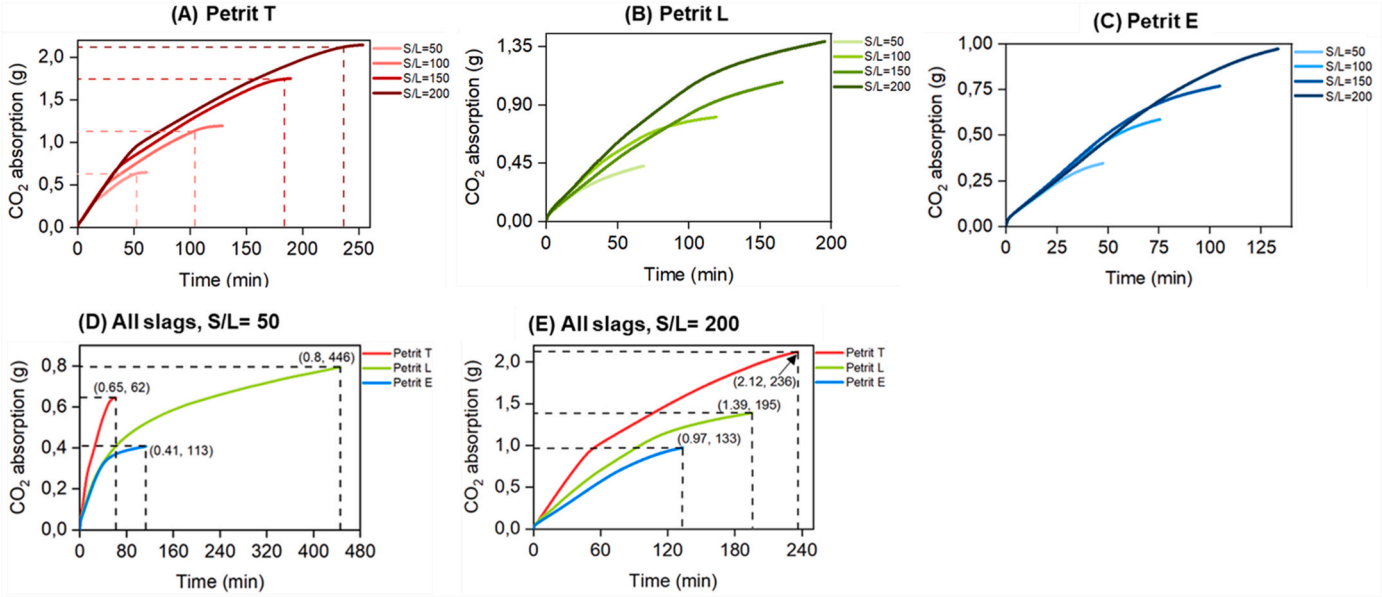

Fig. 5. Absorption of CO_2 for all mixtures of (A) Petrit T, (B) Petrit L and (C) Petrit E, where the dashed lines in (A) correspond to 14% CO_2 in the outlet, as well as comparison between the different slags for (D) S/L = 50 and (E) S/L = 200.

flows into the mixture the pH drops and the $MgCO_3$ starts to turn into Mg $(HCO_3)_2$ which is water soluble and thus leaching into the water leaving the surface of the MgO uncovered so that more of it can react.

Petrit E, which also contains MgO displayed a similar performance as Petrit L. It did not take such a long time, but it did display very slow carbonation after the gas outlet reached 14% of CO_2. For these two materials, for the sake of reducing the experiments to more manageable durations, the rest of the mixtures (S/L = 100–200) were carbonated until the gas outlet reached 14% CO_2 concentration.

To investigate the contribution of leached metal ions coming from the pretreatment to the overall carbonation process, mixtures of S/L = 50 were prepared for all the steel slags by stirring for 24 h and then isolating the liquid medium via centrifugation. The carbonation evolution of the supernatant samples is displayed in Fig. 4. The total absorption of the supernatant solutions was around 0.11, 0.08 and 0.06 g of CO_2 for the Petrit T (Fig. 4A), L (Fig. 4B) and E (Fig. 4C) respectively. This accounts for 17%, 10% and 15% of the total absorption in the mixtures of Petrit T, L and E, respectively. Due to the low solubility of Ca^{2+} the aqueous media reach their saturation levels at quite low concentrations. Thus, after stirring for 24 h, most metals which can react with CO_2 towards carbonation are still inside the materials in solid form. Nevertheless, the authors believe that the stirring pretreatment enhances the wetting of the solids, allowing the metals to be more easily accessible, which contributes towards a fast carbonation process without the requirement for intense operating conditions, such as high pressure. The curves of pH in Fig. 4 were significantly smoother than those in Fig. 3, supporting the theory that the irregularities in the pH curves of Fig. 3 stem from the shifts in equilibrium between the solid and aqueous Ca as the carbonation progresses.

3.3. Carbonation performance for mixtures of different S/L ratios

Fig. 5 shows the absorption of CO_2 in all slags and at all S/L ratios. It can be observed in Fig. 5A, B and C that for all the slags higher S/L ratio resulted in higher absorption of CO_2. This was expected as higher amount of solids in water means that there are more metal oxides available to react with CO_2. Fig. 5D displays the CO_2 absorption of the three slags at S/L = 50, where, as mentioned before, the carbonation was

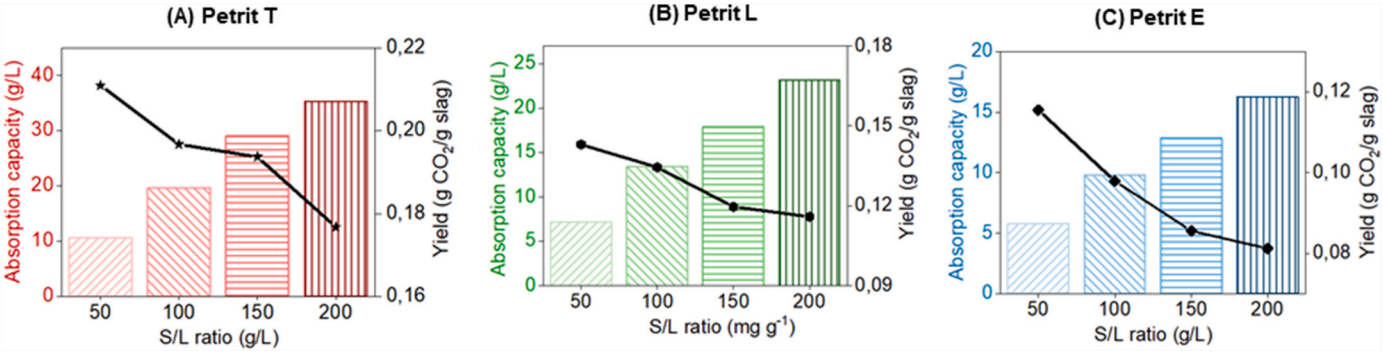

Fig. 6. Absorption capacities and yield for: (A) Petrit T; (B) Petrit L; (C) Petrit E. The bar data correspond to the absorption capacity and the line graphs correspond to the yield of carbonation.

carried on until the outlet CO_2 matched the inlet. The Figure shows that Petrit T had a higher rate of absorption. Petrit L and E had similar absorption rates at the beginning, but while Petrit E diverged and slowed down, displaying the lowest total absorption, Petrit L carried on leading to the highest total absorption of the three. If the goal of the process was to fully carbonate the materials perhaps it could be chosen to opt for very long operation times for the Petrit L and E, which would also lead to high carbon capture. However, if the purpose is to design a system for CO_2 absorption, it would be more beneficial to select shorter process times, which will lead to partial carbonation of the material. Looking at the CO_2 absorption of the S/L = 200 mixtures (Fig. 5E), which went on until 14% CO_2 in the outlet, it is easier to conclude that Petrit T is the leading material in terms of absorption capacity and reaction times.

3.4. Absorption capacity versus yield of carbonation

The comparison between the absorption capacity and carbonation yield of the steelmaking slags is displayed in Fig. 6. As mentioned before the absorption capacity increases with increasing S/L ratio. However, the yield of carbonation follows an opposite trend, meaning that with increasing S/L ratio the carbonation of the solids decreases. This is related to the equilibrium between dissolved and solid metals in the mixtures. At high S/L ratios, the Ca^{2+} ions saturate the water quickly and act competitively against the rest of the Ca^{2+} in the material. As CO_2 is introduced it may react with the CaO in solid form, creating an insoluble layer of $CaCO_3$ on the surface of the solid particles, hindering the leaching of more metal ions. This result draws emphasis to the particle size, as the slag with the lowest particle size (Petrit T) was shown to have the highest absorption capacities for all S/L ratios. Smaller particle size increases the surface of the solids, thus allowing more metal ions to leach out and react with CO_2.

This suggests that the S/L ratio is a crucial parameter when designing a large-scale process. On the one hand, lower S/L ratio allows for better utilization of the materials. Thus, if the purpose of the process was to obtain enhanced, carbonated steel slags, then the S/L = 50 could be preferred. But, on the other hand, it must be considered that lower S/L ratio entails higher reactor volumes, hence leading to extra costs. If an industrial process were to be designed for the purpose of treating flue gas to remove most of its CO_2 content, then several in-line reactors could be used to capture as much of the CO_2 as possible. In such a process the in-line reactors could contain mixtures of rising S/L ratio, starting from 50 in the first one and increasing to more potent mixtures to counteract the lower concentration of CO_2 entering each reactor. This, however, is only a speculation and further optimization is required to obtain the best performing system depending on the purpose of the application.

3.5. Physicochemical characterization

The solid particles formed during the reaction were analyzed by solid state FTIR, XRD and SEM. The analysis of samples with S/L ratio 150 is displayed below. This ratio was chosen as it is near the middle of the S/L ratio range tested. Physicochemical characterization was also conducted for the samples of S/L 50 and 200, but they did not display significant differences. It must be noted that the solid powders analyzed were the ones dispersed in the solution. During the preparation of the solutions, big solid particles (stone-like shapes) were observed in the bottom of the

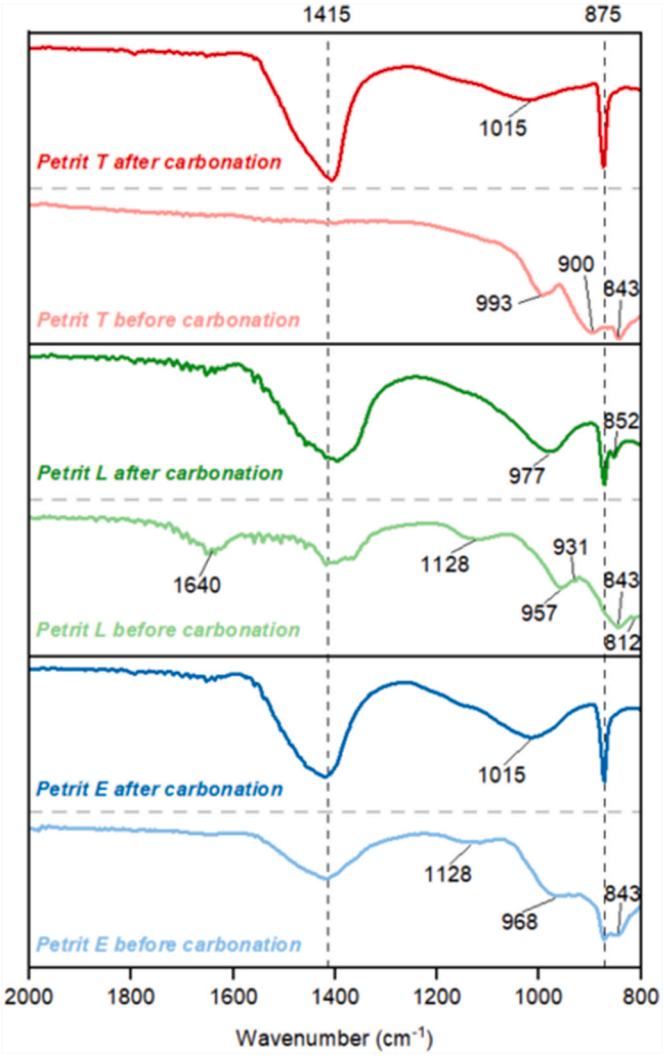

Fig. 7. FTIR of solid powders (experiment at S/L = 150) for Petrit T, Petrit L and Petrit E.

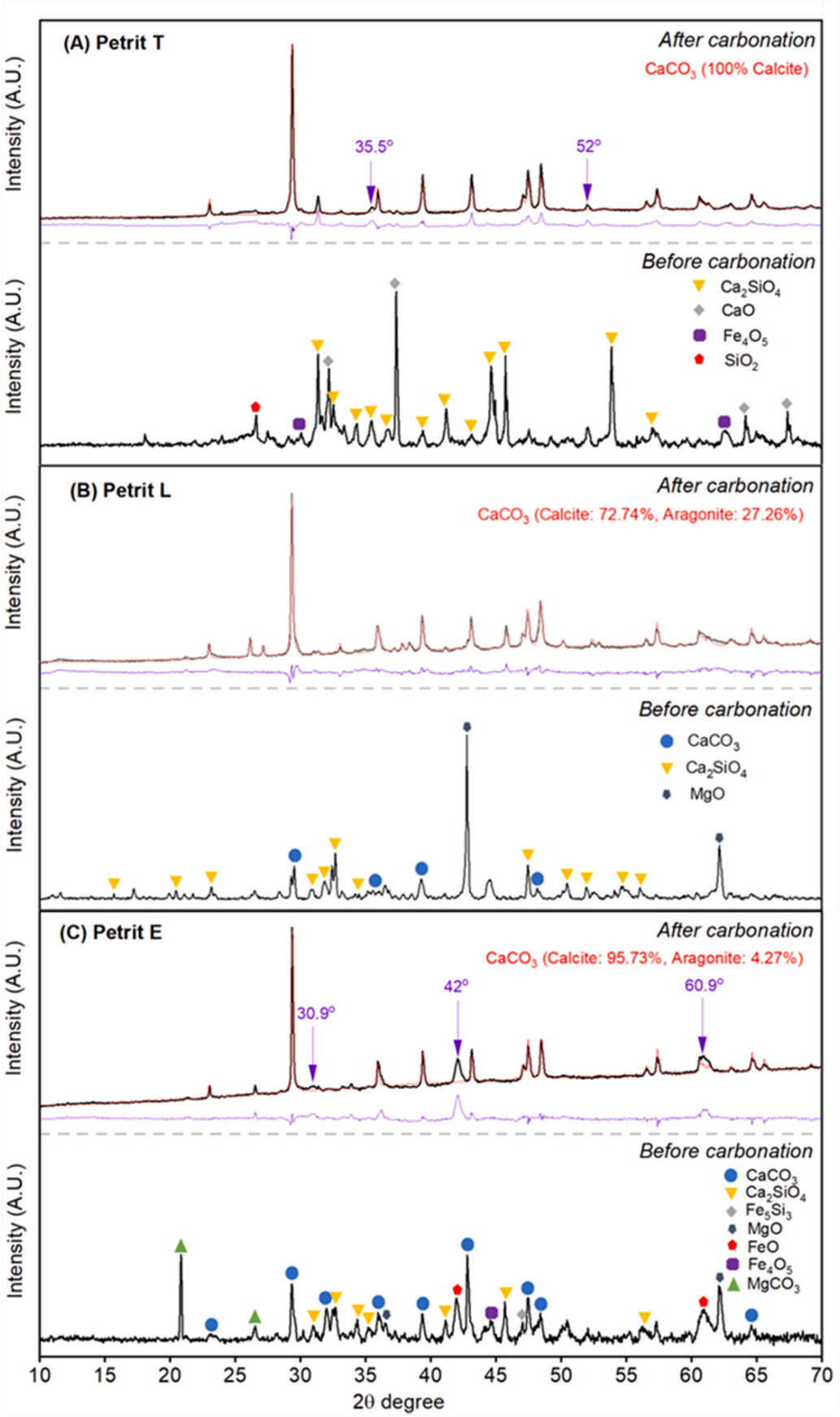

Fig. 8. XRD of solid powders (experiment at S/L = 150) before and after carbonation for: (A) Petrit T; (B) Petrit L; (C) Petrit E. The experimental curves are represented in black, the calculated data in red and the difference between them is in purple.

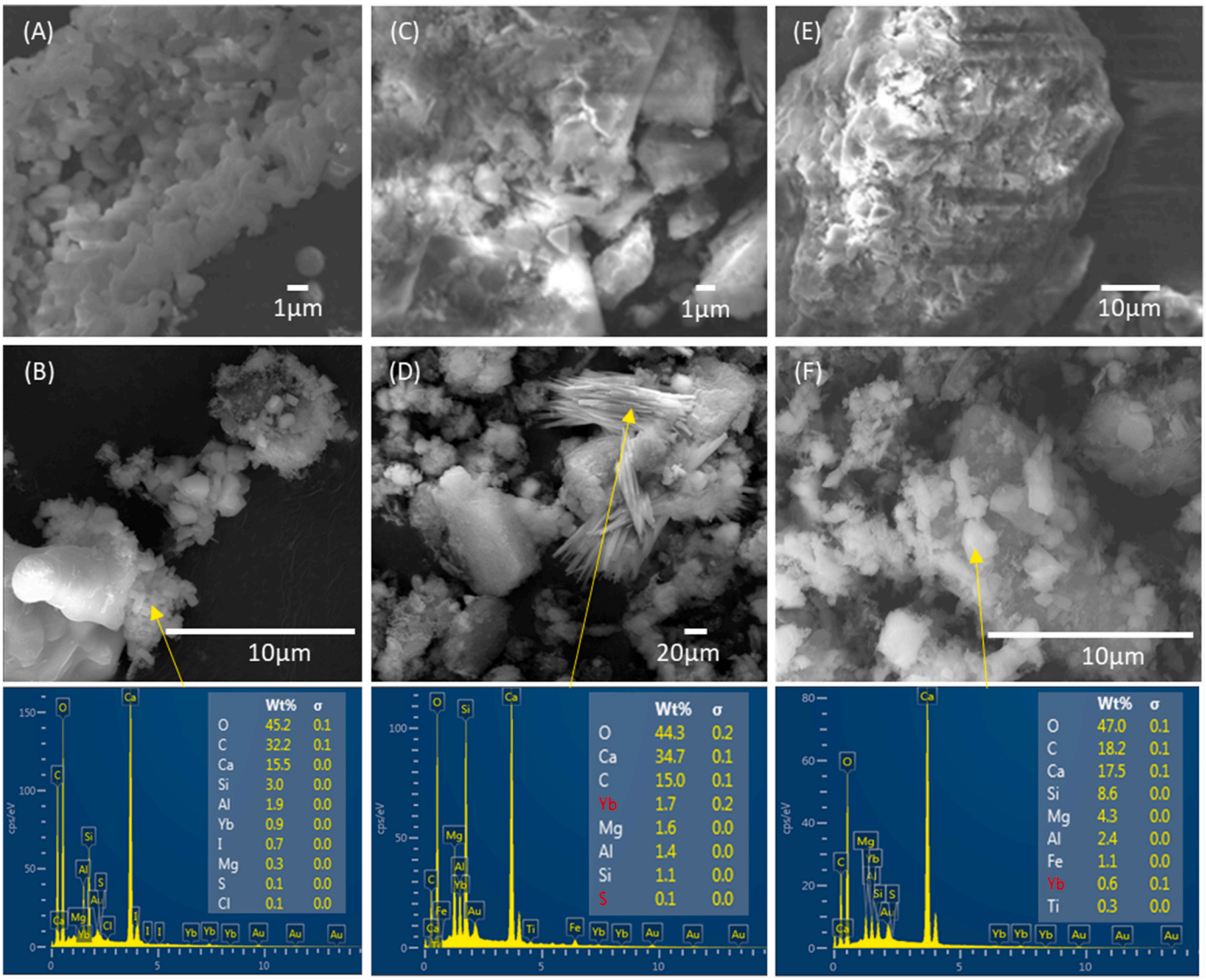

Fig. 9. SEM of solid powders for: (A) Petrit T before carbonation; (B) Petrit T after carbonation; (C) Petrit L before carbonation; (D) Petrit L after carbonation; (E) Petrit E before carbonation; (F) Petrit E after carbonation. The carbonated samples are the ones from the experiment at S/L = 150. The EDS analysis is shown on the right of the images. Small peaks of Au appeared due to the Au coating on the samples.

reactor. These solids were assumed to be a side stream of the reaction and its analysis is out of scope.

Fig. 7 shows the FTIR spectra of the steel slags before and after carbonation. The intense peaks at around 1415 cm^{-1} and 875 cm^{-1} which appeared after carbonation correspond to the asymmetric stretching and out-of-place bending of CO_3^{2-}, respectively (Salman et al., 2015). In fact, very similar spectra were obtained in previous works for $CaCO_3$ analysis (Baena-Moreno et al., 2019a,b,c). This fact confirms a high presence of carbonate in the solid formed, opening new potential paths for utilization of the powders. Small peaks of the Si–O, Al–O and aluminosilicate bonds could also be distinguished in the spectra. The peaks at 812, 900 and 931 cm^{-1} could belong to Si–O stretching of Q^1 tetrahedra and the peaks at around 957, 968 and 977 cm^{-1} might correspond to the Si–O Q^2 bond (Yu et al., 1999). The peaks that appeared at 843 and 852 could potentially belong to the Al–O bond and the broad band at around 1015 cm^{-1} has been found to belong to Si–O–Al (Yusuf, 2023). The small peak at around 1640 cm^{-1} in Petrit L before carbonation belongs to water (Yu et al., 1999). Petrit L and E before carbonation also displayed a small band at around 1128 cm^{-1}, which might belong to the Si–O Q^3 bond (Yu et al., 1999). After carbonation, the small peaks of Si–O bonds were lost due to the strong signal coming from the carbonates. However, the aluminosilicate band at 1015 cm^{-1} could be distinguished in Petrit T and E. We could speculate that this band arises because some of the Ca that initially existed in silicate complexes leached and formed $CaCO_3$ leaving an excess of Si and thus promoting the formation of more aluminosilicate bonds. An intense peak of the Si–O bond at 977 cm^{-1} and a shoulder of the Al–O bond (852 cm^{-1}) were also visible in the Petrit L sample after carbonation.

Once confirmed by FTIR that the predominant species are carbonates (most probably $CaCO_3$), it is important to investigate the crystal polymorphs of the solid powders. To this end, XRD was used. XRD is not only useful to identify different carbonate species (i.e., $CaCO_3$ or $MgCO_3$), but also to distinguish different crystal polymorph forms. For example, in the case of $CaCO_3$, three main crystal polymorphs form: calcite, aragonite, and vaterite (Baena-Moreno et al., 2019b). Fig. 8 shows the X-ray diffraction patterns of the slags before and after carbonation. As can be seen at first sight, quite different results were obtained for the different slags. For example, for Petrit T (Fig. 8A) the sample before carbonation displayed patterns characteristic of Ca_2SiO_4 and CaO, as well as other structures. Petrit L and E had peaks characteristic of Ca_2SiO_4, $CaCO_3$ and MgO before carbonation (Fig. 8B and C). After carbonation, the

crystalline phases present in the materials were analyzed by Rietveld refinement. The major crystalline phase present in Petrit T after carbonation was calcite, as can be seen in Fig. 8A (Tyutyunnik et al., 2003). However, two very low-intensity, unfitted peaks were also present near 35.5 and 52 2Θ degrees. The peak at 35.5 2Θ degrees could belong to Fe_3O_4 according to the Crystallography Open Database. The peak at 52 2Θ degrees could not be identified. The peaks present in the diffractogram of Petrit L after carbonation belonged only to $CaCO_3$ polymorphs (Fig. 8B). The two contributing polymorphs were found to be calcite and aragonite with 72.74% and 27.26%, respectively. Lastly, in carbonated Petrit E, $CaCO_3$ was also the predominant phase, as can be seen in Fig. 8C. It was mainly in the form of calcite, with a contribution of 95.73%, but a small percentage of aragonite (4.27%) was present as well. This analysis was challenging due to the existence of three peaks, which could not be fitted at 30.9, 42 and 60.9 2Θ degrees. The peak near 30.9 2Θ degrees could belong to dolomite ($CaMg(CO_3)_2$) and the other two could be attributed to FeO. This is a very encouraging result since the predominance of calcite could allow utilization of the materials for example for volume substructure in order to create stable conditions for subsequent land constructions and buildings. Another area of use is as materials for road construction or aggregates in asphalt (Baena-Moreno et al., 2020; Sorrentino et al., 2023).

Further physicochemical information on the morphology of the solid samples was obtained with SEM, as shown in Fig. 9. The morphology of the samples before carbonation (Fig. 9A–E) is different among the virgin slags. For example, a sponge-like morphology was observed for Petrit T, while a rock-alike shape was found for Petrit E. Nonetheless, for the carbonated samples, we saw more similar morphologies than for the raw ones. According to previous references, calcite presents a tetrahedral morphology. This morphology can be seen in Fig. 9B (Petrit T carbonated) and Fig. 9F (Petrit E carbonated) (Baena-Moreno et al., 2019b). EDS analysis showed a high content of Ca in these structures, confirming that they are most probably calcite. Small amounts of Si, Mg, Al and Fe were also detected on the crystals, suggesting that the formed calcite is not pure, which is expected given the complex composition of the slags. For the carbonated sample of Petrit L, a mix of tetrahedral- and needle-alike morphology was observed (Fig. 9D). EDS showed that the needle structures had a high content of Ca and thus, in accordance with the Rietveld refinement these structures could be identified as aragonite. These results match with the FTIR and XRD analysis, hence validating the overall physicochemical characterization performed.

4. Conclusions

In this work, we evaluated the mineral carbonation potential of three industrial steel slag via aqueous carbonation. To this end, we studied the absorption capacities, yields, and physicochemical characteristics of the carbonated samples. In agreement with the results obtained, we can conclude the following facts: (1) Petrit L had the highest absorption capacity, but it was reached at a very slow rate; (2) Petrit T presented the best performance in terms of CO_2 absorption rate, while Petrit E was the worst performing out of the three both in absorption rate and capacity; (3) For all the slags, the absorption capacities increase with the increase in S/L ratio, with values between 5.8 and 35.3 g/L; (4) The yields follow an opposite trend (values in the range 81–211 kg CO_2/ton of slag), meaning that we can make better use of the slags with low S/L ratio, but this would require larger reactor volumes; (5) The physicochemical characterization of the solid product indicated $CaCO_3$ was a major product of the carbonation, suggesting that there is potential to use this carbonated product in commercial applications.

All in all, our results can help to gain some insights into the carbonation potential of different steel slags in processes with low energy consumption. Nonetheless, further future work must be carried out to have the knowledge needed to scale up the process. In this line, future works could explore the use of spatially resolved techniques for example magnetic resonance imaging to gain insights into the kinetics of the process as well as on the mixing and flow patterns that happen during the reaction. This could help to obtain valuable data for developing robust computational fluid dynamics models which will be helpful to optimize reactions and process design.

CRediT authorship contribution statement

Emmanouela Leventaki: Writing – review & editing, Visualization, Methodology, Investigation, Formal analysis, Conceptualization. **Eduarda Couto Queiroz:** Writing – review & editing, Visualization, Investigation. **Shyam Krishnan Pisharody:** Investigation. **Amit Kumar Siva Kumar:** Investigation. **Phuoc Hoang Ho:** Writing – review & editing, Investigation. **Michael Andersson-Sarning:** Methodology. **Björn Haase:** Writing – review & editing, Conceptualization. **Francisco M. Baena-Moreno:** Writing – review & editing, Writing – original draft, Visualization, Supervision, Project administration, Methodology, Investigation, Funding acquisition, Conceptualization. **Alexandre Cuin:** Formal analysis. **Diana Bernin:** Writing – review & editing, Supervision, Project administration, Methodology, Funding acquisition, Conceptualization.

Declaration of competing interest

The authors declare that they have no known competing financial interests or personal relationships that could have appeared to influence the work reported in this paper.

Data availability

Data will be made available on request.

Acknowledgments and Funding

We acknowledge the Area of Advance Energy, Chalmers University of Technology and Energimyndigheten (P2021-00009) for financial support. Authors thank Nordic DAC Group's in-kind contribution in sourcing suitable material from industry partners/Höganäs. Authors also thank Carl Tryggers Stiftelse för Vetenskaplig Forskning for providing funding with the project "Instrumentation to utilise research on CO_2 capture to reach the climate goals".

References

Altomare, A., Corriero, N., Cuocci, C., Falcicchio, A., Moliterni, A., Rizzi, R., n.d. QualX Version 2.24 ..

Baciocchi, R., Costa, G., Di Bartolomeo, E., Polettini, A., Pomi, R., 2010. Carbonation of stainless steel slag as a process for CO2 storage and slag valorization. Waste Biomass Valorization 1, 467–477. https://doi.org/10.1007/s12649-010-9047-1.

Baena-Moreno, F.M., Cid-Castillo, N., Arellano-García, H., Reina, T.R., 2021. Towards emission free steel manufacturing – exploring the advantages of a CO2 methanation unit to minimize CO2 emissions. Sci. Total Environ. 781, 146776 https://doi.org/10.1016/j.scitotenv.2021.146776.

Baena-Moreno, F.M., Leventaki, E., Riddell, A., Wojtasz-Mucha, J., Bernin, D., 2022. Effluents and residues from industrial sites for carbon dioxide capture: a review. Environ. Chem. Lett. https://doi.org/10.1007/s10311-022-01513-x.

Baena-Moreno, F.M., Price, C.A., le Saché, E., Pastor-Pérez, L., Sebastia-Saez, D., Reina, T.R., 2019a. Physicochemical comparison of precipitated calcium carbonate for different configurations of a biogas upgrading unit. J. Chem. Technol. Biotechnol. JCTB 6013. https://doi.org/10.1002/jctb.6013.

Baena-Moreno, F.M., Rodríguez-Galán, M., Reina, T.R., Zhang, Z., Vilches, L.F., Navarrete, B., 2019b. Understanding the effect of Ca and Mg ions from wastes in the solvent regeneration stage of a biogas upgrading unit. Sci. Total Environ. 691, 93–100. https://doi.org/10.1016/j.scitotenv.2019.07.135.

Baena-Moreno, F.M., Rodríguez-Galán, M., Vega, F., Reina, T.R., Vilches, L.F., Navarrete, B., 2019c. Synergizing carbon capture storage and utilization in a biogas upgrading lab-scale plant based on calcium chloride: influence of precipitation parameters. Sci. Total Environ. 670, 59–66. https://doi.org/10.1016/j.scitotenv.2019.03.204.

Baena-Moreno, F.M., Vega, F., Pastor-Pérez, L., Reina, T.R., Navarrete, B., Zhang, Z., 2020. Novel process for carbon capture and utilization and saline wastes valorization. J Nat Gas Sci Eng 73, 103071. https://doi.org/10.1016/j.jngse.2019.103071.

Bonenfant, D., Kharoune, L., Sauve′, S., Hausler, R., Niquette, P., Mimeault, M., Kharoune, M., 2008. CO $_2$ sequestration potential of steel slags at ambient pressure and temperature. Ind. Eng. Chem. Res. 47, 7610–7616. https://doi.org/10.1021/ie701721j.

The Engineering ToolBox (2018). *Carbon dioxide - Density and Specific Weight vs. Temperature and Pressure*. [online] Available at: https://www.engineeringtoolbox.com/carbon-dioxide-density-specific-weight-temperature-pressure-d_2018.html. (Accessed 12 September 2023).

Chang, E.-E., Pan, S.-Y., Chen, Y.-H., Tan, C.-S., Chiang, P.-C., 2012. Accelerated carbonation of steelmaking slags in a high-gravity rotating packed bed. J. Hazard Mater. 227–228, 97–106. https://doi.org/10.1016/j.jhazmat.2012.05.021.

Gerres, T., Lehne, J., Mete, G., Schenk, S., Swalec, C., 2021. Green Steel Production: How G7 Countries Can Help Change the Global Landscape [WWW Document]. Leadership group for industry transition. URL. https://www.industrytransition.org/insights/g7-green-steel-production/, 3.14.23.

Ghacham, A. Ben, Pasquier, L.-C., Cecchi, E., Blais, J.-F., Mercier, G., 2016. CO2 sequestration by mineral carbonation of steel slags under ambient temperature: parameters influence, and optimization. Environ. Sci. Pollut. Control Ser. 23, 17635–17646. https://doi.org/10.1007/s11356-016-6926-4.

González-Arias, J., González-Castaño, M., Sánchez, M.E., Cara-Jiménez, J., Arellano-García, H., 2022. Valorization of biomass-derived CO2 residues with Cu-MnOx catalysts for RWGS reaction. Renew. Energy 182, 443–451. https://doi.org/10.1016/j.renene.2021.10.029.

Han, S.-J., Yoo, M., Kim, D.-W., Wee, J.-H., 2011. Carbon dioxide capture using calcium hydroxide aqueous solution as the absorbent. Energy Fuels 25, 3825–3834. https://doi.org/10.1021/ef200415p.

Ho, H.-J., Iizuka, A., Shibata, E., 2021. Utilization of low-calcium fly ash via direct aqueous carbonation with a low-energy input: determination of carbonation reaction and evaluation of the potential for CO2 sequestration and utilization. J. Environ. Manag. 288, 112411 https://doi.org/10.1016/j.jenvman.2021.112411.

HYBRIT, 2023. HYBRIT fossil-free steel [WWW Document]. URL. https://www.hybritdevelopment.se/en/, 3.14.23.

International Energy Agency, 2022. Iron and Steel.

Kim, A.G., Kazonich, G., 2004. The Silicate/non-silicate distribution of metals in fly ash and its effect on solubility. Fuel 83, 2285–2292. https://doi.org/10.1016/J.FUEL.2004.06.005.

Lekakh, S.N., Rawlins, C.H., Robertson, D.G.C., Richards, V.L., Peaslee, K.D., 2008. Kinetics of aqueous leaching and carbonization of steelmaking slag. Metall. Mater. Trans. B 39, 125–134. https://doi.org/10.1007/s11663-007-9112-8.

Li, L., Ling, T.-C., Pan, S.-Y., 2022. Environmental benefit assessment of steel slag utilization and carbonation: a systematic review. Sci. Total Environ. 806, 150280 https://doi.org/10.1016/j.scitotenv.2021.150280.

Li, T., Keener, T.C., Cheng, L., 2014. Carbon dioxide removal by using $Mg(OH)_2$ in a bubble column: effects of various operating parameters. Int. J. Greenh. Gas Control 31, 67–76. https://doi.org/10.1016/j.ijggc.2014.09.027.

Liu, J., Wang, Z., Xie, G., Li, Z., Fan, X., Zhang, W., Xing, F., Tang, L., Ren, J., 2022a. Resource utilization of municipal solid waste incineration fly ash - cement and alkali-activated cementitious materials: a review. Sci. Total Environ. 852, 158254 https://doi.org/10.1016/j.scitotenv.2022.158254.

Liu, Y., Zhuge, Y., Fan, W., Duan, W., Wang, L., 2022b. Recycling industrial wastes into self-healing concrete: a review. Environ. Res. 214, 113975 https://doi.org/10.1016/j.envres.2022.113975.

Luo, W., Li, B., Xu, M., Pang, C., Lester, E., Xu, L., Kow, K.-W., 2023. In-situ release and sequestration of CO2 in cement composites using LTA zeolites. Sci. Total Environ. 872, 162133 https://doi.org/10.1016/j.scitotenv.2023.162133.

Luo, Y., He, D., 2021. Research status and future challenge for CO2 sequestration by mineral carbonation strategy using iron and steel slag. Environ. Sci. Pollut. Control Ser. 28, 49383–49409. https://doi.org/10.1007/s11356-021-15254-x.

Pan, S.-Y., Chiang, P.-C., Chen, Y.-H., Tan, C.-S., Chang, E.-E., 2013. Ex situ CO $_2$ capture by carbonation of steelmaking slag coupled with metalworking wastewater in a rotating packed bed. Environ. Sci. Technol. 47, 3308–3315. https://doi.org/10.1021/es304975y.

Paufler, P., 1995, 494–494. In: Young, R.A. (Ed.), The Rietveld Method. International Union of Crystallography, vol. 30. Oxford University Press. https://doi.org/10.1002/crat.2170300412, 1993. 298 pp. Price £ 45.00. ISBN 0–19–855577–6. Crystal Research and Technology.

Ragipani, R., Bhattacharya, S., Suresh, A.K., 2021. A review on steel slag valorisation via mineral carbonation. React. Chem. Eng. 6, 1152–1178. https://doi.org/10.1039/D1RE00035G.

Sabri, M.A., Al Jitan, S., Bahamon, D., Vega, L.F., Palmisano, G., 2021. Current and future perspectives on catalytic-based integrated carbon capture and utilization. Sci. Total Environ. 790, 148081 https://doi.org/10.1016/j.scitotenv.2021.148081.

Salman, M., Cizer, Ö., Pontikes, Y., Snellings, R., Vandewalle, L., Blanpain, B., Balen, K. Van, 2015. Cementitious binders from activated stainless steel refining slag and the effect of alkali solutions. J. Hazard Mater. 286, 211–219. https://doi.org/10.1016/j.jhazmat.2014.12.046.

Sorrentino, G.P., Zanoletti, A., Ducoli, S., Zacco, A., Iora, P., Invernizzi, C.M., Di Marcoberardino, G., Depero, L.E., Bontempi, E., 2023. Accelerated and natural carbonation of a municipal solid waste incineration (MSWI) fly ash mixture: Basic strategies for higher carbon dioxide sequestration and reliable mass quantification. Environ Res 217, 114805. https://doi.org/10.1016/j.envres.2022.114805.

TOPAS-R, Version 4.2, 2009. General Profile and Structure Analysis Software for Powder Diffraction Data.

Tyutyunnik, A.P., Slobodin, B.V., Samigullina, R.F., Verberck, B., Tarakina, N.V., 2003. Dalton Trans.

Wang, Y., Pan, Z., Zhang, W., Borhani, T.N., Li, R., Zhang, Z., 2022. Life cycle assessment of combustion-based electricity generation technologies integrated with carbon capture and storage: a review. Environ. Res. 207, 112219 https://doi.org/10.1016/j.envres.2021.112219.

Yagmur Goren, A., Erdemir, D., Dincer, I., 2024. Comprehensive review and assessment of carbon capturing methods and technologies: an environmental research. Environ. Res. 240, 117503 https://doi.org/10.1016/j.envres.2023.117503.

Yang, S., Mo, L., Deng, M., 2021. Effects of ethylenediamine tetra-acetic acid (EDTA) on the accelerated carbonation and properties of artificial steel slag aggregates. Cem. Concr. Compos. 118, 103948 https://doi.org/10.1016/J.CEMCONCOMP.2021.103948.

Yu, P., Kirkpatrick, R.J., Poe, B., McMillan, P.F., Cong, X., 1999. Structure of calcium silicate hydrate (C-S-H): near-, mid-, and far-infrared spectroscopy. J. Am. Ceram. Soc. 82, 742–748. https://doi.org/10.1111/j.1151-2916.1999.tb01826.x.

Yusuf, M.O., 2023. Bond characterization in cementitious material binders using Fourier-transform infrared spectroscopy. Appl. Sci. 13, 3353. https://doi.org/10.3390/app13053353.

Zhao, Q., Chu, X., Mei, X., Meng, Q., Li, J., L iu, C., Saxén, H., Zevenhoven, R., 2020. Co-Treatment of waste from steelmaking processes: steel slag-based carbon capture and storage by mineralization. Front. Chem. 8 https://doi.org/10.3389/fchem.2020.571504.